

Induced chiral Dirac fermions in graphene by a periodically modulated magnetic field

Lei Xu,¹ Jin An,¹ and Chang-De Gong^{2,1}

¹National Laboratory of Solid State Microstructures and Department of Physics, Nanjing University, Nanjing 210093, China

²Center for Statistical and Theoretical Condensed Matter Physics,
and Department of Physics, Zhejiang Normal University, Jinhua 321004, China

(Dated: June 16, 2018)

The effect of a modulated magnetic field on the electronic structure of neutral graphene is examined in this paper. It is found that application of a small staggered modulated magnetic field does not destroy the Dirac-cone structure of graphene and so preserves its 4-fold zero-energy degeneracy. The original Dirac points (DPs) are just shifted to other positions in k space. By varying the staggered field gradually, new DPs with exactly the same electron-hole crossing energy as that of the original DPs, are generated, and both the new and original DPs are moving continuously. Once two DPs are shifted to the same position, they annihilate each other and vanish. The process of generation and evolution of these DPs with the staggered field is found to have a very interesting pattern, which is examined carefully. Generally, there exists a corresponding branch of anisotropic massless fermions for each pair of DPs, resulting in that each Landau level (LL) is still 4-fold degenerate except the zeroth LL which has a robust $4n_t$ -fold degeneracy with n_t the number of pairs of DPs. As a result, the Hall conductivity σ_{xy} shows a step of size $4n_t e^2/h$ across zero energy.

PACS numbers: 73.43.Cd, 73.22.Pr, 73.61.Wp

Low energy physics of neutral graphene is characterized by the two inequivalent Dirac cones which is related by the time-reversal symmetry and described by the relativistic massless Dirac equation.^{1,2,3,4} Nearly all important properties of neutral graphene is governed by the chiral massless fermions around the two cones. For example, the zero-energy anomaly due to the linear energy dispersion and the particle-hole symmetry of the Dirac cones give rise to the anomalous quantum Hall effect (QHE)^{3,4,5,6,7,8} or the so-called half-integer QHE, where the Hall conductivity is quantized to be half-integer multiples of $4e^2/h$. When the Dirac-cone topology is destroyed or replaced by other structures, the system will undergo quantum phase transitions. In bilayer graphene, each Dirac cone is replaced by two touching parabolic bands,^{9,10,11} which leads to the 8-fold degeneracy of zero-energy level,⁹ giving rise to the quantized Hall conductivity in bilayer graphene taken on values of integer multiples of $4e^2/h$.^{9,10}

Modulation of electronic structure in graphene has already been experimentally realized, where periodic electronic^{12,13} or magnetic^{14,15} potentials can be applied to graphene by making use of substrate^{16,17,18,19} or controlled adatom deposition,²⁰ or by fabrication of periodic patterned gate electrodes. This kind of graphene superlattice potential can change the Dirac-cone structure of graphene dramatically,^{21,22} which may lead to some new phenomena, as well as potential application of graphene materials.

In this paper, we present a study on the electronic structure of monolayer neutral graphene and its unusual integer QHE under the influence of a periodically modulated orbital magnetic field, which is schematically shown in Fig.1. This kind of one-dimensional modulation of magnetic field can be achieved in experiments by applying an array of ferromagnetic stripes with al-

ternative magnetization on the top of a graphene layer, or by making use of cold atoms in a honeycomb optical lattice,^{23,24,25} or “artificial graphene” realized in a nanopatterned two-dimensional electron gas.²⁶ Our analysis shows that generally the Dirac-cone structure can not be smeared out by this time-reversal invariant magnetic field. Similar to the cases of periodic electronic potential,^{21,22} new DPs will be generated with varying the amplitude of the field. What’s remarkable and different is that the newly generated DPs together with the original DPs will move and evolve in k space with the field. This leads to a series of quantum phase transitions with each phase characterized by its unusual integer QHE, which is expected to be observed by Hall measurements.

We start with the tight-binding model on a honeycomb lattice in the presence of a perpendicular, periodically modulated orbital magnetic field. The Hamiltonian is given by,

$$H = -t \sum_{\langle ij \rangle} e^{ia_{ij}} c_i^\dagger c_j + \text{H.c.}, \quad (1)$$

where c_i^\dagger (c_i) is an electron creation (annihilation) operator on site i , and $\langle ij \rangle$ denotes nearest-neighbor pairs of sites. Here the spin index is suppressed since we do not consider the Zeeman splitting. The magnetic flux per hexagon (the summation of a_{ij} along the six bonds around a hexagon) is given by $\sum a_{ij} = \phi \pm \delta$, where ϕ measures the uniform magnetic flux whereas δ the staggered modulated flux, both of which are in units of $\phi_0/2\pi$ with ϕ_0 the flux quantum. Hereafter energy is measured in unit of the nearest-neighbor hopping integral t .

To begin with, let us consider the effect of the two simplest types of staggered magnetic fields (SMFs), in order to extract the main physics behind graphene under the influence of a modulated orbital magnetic field. The

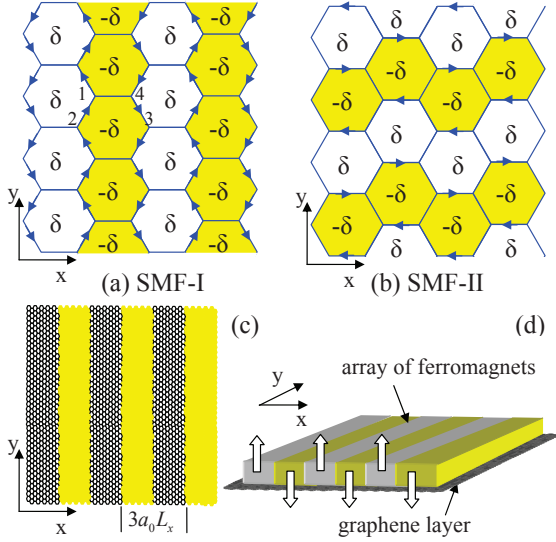


FIG. 1: (Color online) Illustration of the rectangular sample of graphene under periodically modulated magnetic fields. (a) and (b) represent two simplest SMFs, where each white and yellow (grey) hexagon has a flux δ and $-\delta$, respectively. The numbers 1, \dots , 4 represent the inequivalent atoms in a unit cell. Each arrow represents a phase shift suffered by electrons when hopping along the direction, which is $\delta/4$ in case (a), and $\delta/2$ in case (b). (c) represents a long-period staggered flux applied to graphene with lattice period $3a_0L_x$, where a_0 is the lattice constant. (d) is a corresponding experimental layout in which there is an array of ferromagnetic stripes with alternative magnetization on the top of a graphene layer.

configurations of the two types are schematically shown in Fig. 1(a) and (b), respectively, where proper gauge has been chosen for each case.

We first show the evolution of DPs from an analytical calculation for SMF-I shown in Fig. 1(a). The tight-binding Hamiltonian in k -space can be written as

$$\mathcal{H} = \begin{pmatrix} 0 & \gamma_k & 0 & \eta_k \\ \gamma_k^\dagger & 0 & \eta_k^\dagger & 0 \\ 0 & \eta_k & 0 & \gamma_{-k}^\dagger \\ \eta_k^\dagger & 0 & \gamma_{-k} & 0 \end{pmatrix} \quad (2)$$

where $\gamma_k = -2te^{-i\frac{k_x}{2}} \cos(\frac{\sqrt{3}}{2}k_y + \frac{\delta}{4})$ and $\eta_k = -te^{ik_x}$. The Hamiltonian \mathcal{H} determines the energy spectrum of electrons in graphene under SMF-I. The system has a periodicity of 2π as a function of δ due to gauge invariance, so we restrict δ to range from 0 to 2π . The solution to the DPs can be easily obtained: the original DPs located at $k_x = 0$, $\cos(\sqrt{3}k_y) = \frac{1}{2} - \cos\frac{\delta}{2}$, for $0 < \delta < 4\pi/3$, and the newly generated DPs located at $k_x = \pm\pi/3$, $\cos(\sqrt{3}k_y) = -\frac{1}{2} - \cos\frac{\delta}{2}$, for $2\pi/3 < \delta < 2\pi$.

An overall picture of the evolution of DPs in magnetic Brillouin zone (MBZ) under SMF-I is shown in Fig. 2. When $\delta = 0$, the original pair of DPs (red filled circles) are located at $(0, \pm 2\pi/3\sqrt{3})$ [Fig. 2(a)]. As δ increases, the two DPs move against each other along the k_y direction, and eventually they reach the center of MBZ at

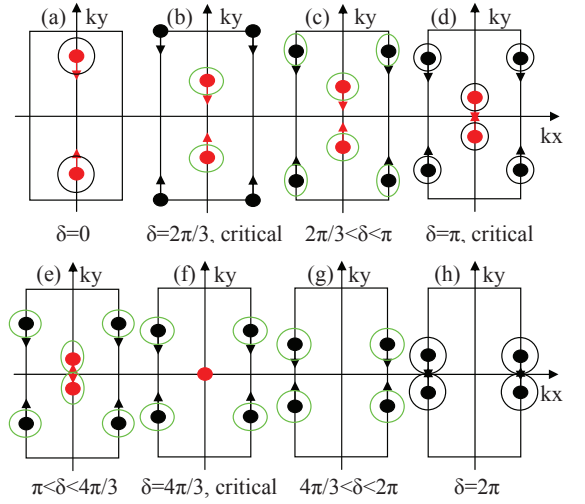


FIG. 2: (Color online) Schematic evolution of DPs in MBZ with increasing staggered flux δ under SMF-I. “●” and “●” represent the original DPs in pristine graphene and the induced (additional) DPs respectively, while the arrows represent their moving directions. The black circles denote isotropic Dirac cones whereas the green (grey) ellipses denote anisotropic Dirac cones. The coordinates of the four corners of MBZ are $(\pm\pi/3, \pm\pi/\sqrt{3})$.

$\delta = 4\pi/3$ [Fig. 2(f)] and thereafter disappear [Fig. 2(g)]. On the other hand, right at $\delta = 2\pi/3$, one additional pair of DPs are induced simultaneously at the four corners of MBZ (see the black filled circles in the figure). Note that only two of the four induced DPs are inequivalent and so only one pair contributes to the system, since the four induced DPs are all located at the boundary of MBZ. With increasing δ the two newly induced DPs move along the lines $k_x = \pm\pi/3$ towards the edge center respectively [Fig. 2(c)-(h)]. When $\delta = 2\pi$, the two DPs arrive at $(\pm\pi/3, \pm 2\pi/3\sqrt{3})$. In this case, electrons hopping along the arrows shown in Fig. 1(a) will suffer an additional phase $\pi/2$, which is a pure gauge. Thus the system corresponding to this value of δ [Fig. 2(h)] is actually physical equivalent to that of Fig. 2(a), because they differ only by a gauge transformation.

It is shown in Fig. 2 that DPs not only annihilate in pairs but also emerge in pairs.²² This is interpreted by the fact that the two DPs in each pair are connected to each other by the time reversal symmetry which is still preserved by the SMF. Now we lay out our numerical results to support these findings. We show for different δ the energy dispersion near zero energy along the two lines $k_x = 0$ [Fig. 3(a)-(e)] and $k_x = \pm\pi/3$ [Fig. 3(f)-(j)] where DPs reside. Note that $\delta = 2\pi/3$ and $4\pi/3$ are two critical values at which the pair of induced DPs emerge and the original DPs completely superpose each other, respectively. Apart from the two critical values, as δ increases from 0 to 2π , the number of DPs changes from one pair to two pairs and then back to one pair. This interesting evolution of DPs will dramatically affect

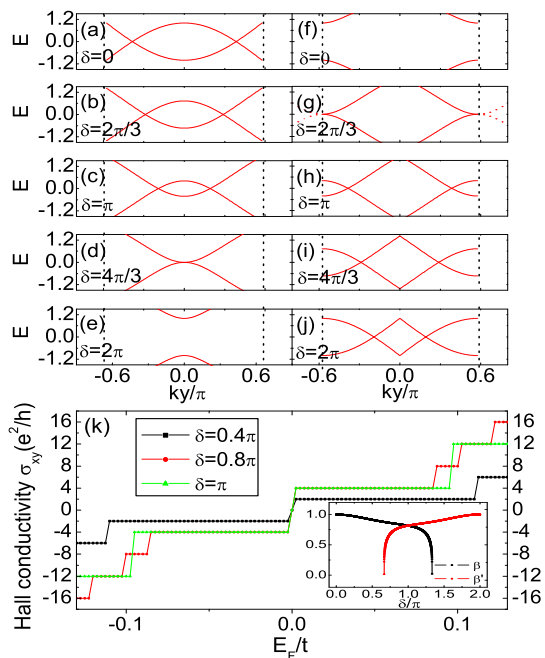


FIG. 3: (Color online) (a)-(e) Electron energy near the DPs under SMF-I versus k_y with $k_x = 0$ for various values of staggered flux δ . The dashed line represents the boundary of MBZ. (f)-(j) The same as (a)-(e) but with $k_x = \pi/3$. (k) Hall conductivity σ_{xy} under SMF-I, with $\phi = 2\pi/768$ for several values of δ . Inset: The two renormalized factors β (β') as functions of staggered flux δ .

the degeneracy of the LLs which can be reflected by the Hall conductivity.

The Hall conductivity can be calculated directly through the standard Kubo formula²⁷ by numerical diagonalization of the Hamiltonian (1). In Fig. 3(k), the resulting Hall conductivity σ_{xy} near zero energy is plotted as a function of the Fermi energy E_F . According to the Hall plateaus steps in σ_{xy} , the system can be classified into three types. For $0 < \delta < 2\pi/3$ or $4\pi/3 < \delta < 2\pi$, with spin degeneracy taken into account, σ_{xy} has a step of size $4e^2/h$, which is the same as that of pristine graphene, shown in Fig. 3(k) for $\delta = 0.4\pi$. For $2\pi/3 < \delta < 4\pi/3$, σ_{xy} has a step of size $8e^2/h$ across zero energy (neutral filling) whereas a step of size $4e^2/h$ in the other energy range, which can be seen in Fig. 3(k) for $\delta = 0.8\pi$. Remarkably, right at $\delta = \pi$, numerical results of Hall conductivity show that all the steps have the same size of $8e^2/h$. We interpret these phenomena as follows.

The isotropic Dirac cones become anisotropic under the influence of a modulated magnetic field (see Fig. 2). The chiral fermions around an anisotropic Dirac cone can be physically described by the anisotropic pseudospin Hamiltonian,

$$\mathcal{H} = v_F \begin{pmatrix} 0 & \hat{p}_- \\ \hat{p}_+ & 0 \end{pmatrix} \quad (3)$$

where $\hat{p}_\pm = a\hat{p}_x \pm ib\hat{p}_y$, $v_F = 3ta_0/2\hbar$ is the Fermi ve-

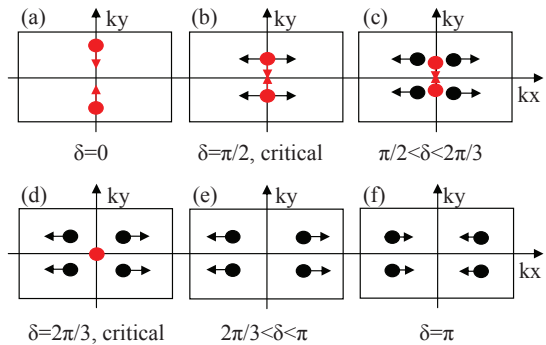


FIG. 4: (Color online) Schematic evolution of DPs in MBZ with increasing staggered flux δ under SMF-II. All symbols used here have the same meanings as that in Fig. 2. The coordinates of the four corners of MBZ are $(\pm\pi/3, \pm\pi/2\sqrt{3})$.

locity, and the two dimensionless coefficients a and b measure the degree of anisotropy of the cone. In the presence of a uniform magnetic field B this anisotropy gives rise to a renormalized LLs $E_n = \pm\beta\hbar v_F \sqrt{|n|/l_B}$ with $\beta = \sqrt{ab}$ a dimensionless renormalization factor, and $l_B = \sqrt{\phi_0/4\pi B}$ the magnetic length. With spin degeneracy taken into account, it is found that for $0 < \delta < 4\pi/3$, the 4-fold degenerate LL spectrum near the original Dirac cones have a β value given by $\beta = \beta(\delta) = \left\{ \frac{2}{\sqrt{3}} \frac{1}{1+\cos(\delta/2)} \left(\frac{1+2\cos(\delta/2)}{3-2\cos(\delta/2)} \right)^{\frac{1}{2}} \right\}^{\frac{1}{2}}$ (note when $\delta = 0$, $\beta = 1$), while for $2\pi/3 < \delta < 2\pi$, the 4-fold degenerate LL spectrum near the induced Dirac cones have another different β' value given by $\beta' = \beta(2\pi - \delta)$. For a general δ between $2\pi/3$ and $4\pi/3$, the LLs for the two branches are not degenerate except the zeroth LL, which is exactly 8-fold degenerate. The zeroth LL is independent of the external uniform magnetic field so its 8-fold degeneracy cannot be removed, leading to a $8e^2/h$ Hall conductivity step at the zeroth LL and a $4e^2/h$ step at other LLs. However, when $\delta = \pi$, the two factors are equal to each other, i.e., $\beta = \beta'$, all LLs for these cones (which are isotropic now) overlap and so are exactly 8-fold degenerate. Therefore at $\delta = \pi$, the Hall conductivity can be expressed as $\sigma_{xy} = 8(N + 1/2)e^2/h$, with N LL index. We remark that actually, within the range of δ where the two pairs of Dirac cones coexist, there should exist a series of critical values of δ given by $\beta^2/\beta'^2 = p/q$, where p and q are two coprime integers. At these critical values, besides the zeroth LL, the m qth LL (with $m = 0, 1, 2, \dots$) in the original pair of cones are exactly degenerate with the m pth LL in the induced pair of cones, giving rise to a $8e^2/h$ Hall conductivity step at these energies. Another critical value of δ is at $\delta = 4\pi/3$, where the zero point at $k_x = k_y = 0$ is not a DP, but rather a semi-DP. Around the semi-DP, energy dispersion is found to be linear along k_x , but parabolic along k_y . This peculiar feature can be compared with the electronic structure in $\text{VO}_2\text{-TiO}_2$ nanoheterostructures.²⁸

Now we turn to explore the second type of the SMF shown in Fig. 1(b). Fig. 4 shows the schematic picture

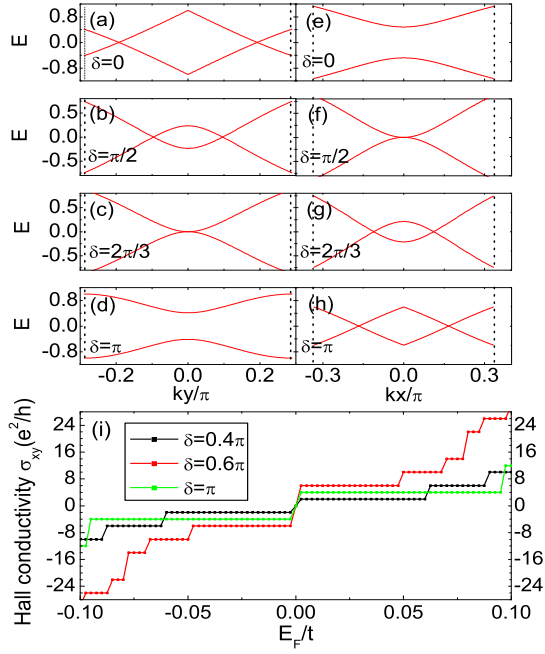


FIG. 5: (Color online) (a)-(d) Electron energy near the DPs under SMF-II, as a function of k_y with $k_x = 0$ for various values of staggered flux δ . The dashed lines represent the boundary of MBZ. (e)-(h) The same as (a)-(d) but as a function of k_x with $k_y = \pi/6\sqrt{3}$, instead. (i) Hall conductivity σ_{xy} under SMF-II with $\phi = 2\pi/768$ for several values of δ .

of the evolution of DPs in the corresponding MBZ. Like that of SMF-I, at the beginning of varying δ , the two DPs of pristine graphene are located at $(0, \pm\pi/3\sqrt{3})$, and then they move towards the origin along k_y direction. When $\delta = \pi/2$, each DP of the pair changes into three DPs at $k=(0, \pm\pi/6\sqrt{3})$ [Fig. 4(b)], but they completely superpose each other and can not be distinguished there. After that the original DPs go on moving along k_y direction and eventually arrive at the origin at $\delta = 2\pi/3$ and then vanish, whereas the other two pairs of induced DPs move along the $k_y = \pm\pi/6\sqrt{3}$ direction until $\delta = \pi$ they reach the points $(\pm\pi/6, \pm\pi/6\sqrt{3})$ [Fig. 4(f)], and then backtrack. The evolution of DPs from $\delta = \pi$ to 2π is just the reverse of the above process.

Compared with the SMF-I, in a period of δ , there are four critical values ($\delta = \pi/2, 2\pi/3, 4\pi/3$, and $3\pi/2$), at which the DPs emerge or vanish. All the induced DPs under SMF-I move parallel to the k_y axis while that under SMF-II move parallel to the k_x axis. This should be associated with the configuration of the SMF, where the induced DPs incline to move towards the periodic direction of the SMF.

The electronic energy spectrum near the zero energy are shown in Fig. 5(a)-(h). What is significant is that as δ increasing from 0 to π , the number of DPs changes from one pair to three pairs and then to two pairs. So, the DPs indeed emerge and annihilate in pairs. In Fig. 5(i), the Hall conductivity σ_{xy} is plotted as a func-

TABLE I: The evolution properties of DPs in MBZ at $0 < \delta < 2\pi/L_x$ for various L_x 's (L_x is from 2 to teens).

SMF δ	L_x	n_o^a (pairs)	n_i^b (pairs)	n_t^c (pairs)
$0 \leq \delta < \delta_c^d$	2	1	0,2	1,3
	3	1	0,2,3	1,3,4
	4	1	0,2,4	1,3,5
	5	1	0,2,4,5	1,3,5,6
	6	1	0,2,4,6	1,3,5,7
	7	1	0,2,4,6,7	1,3,5,7,8
	8	1	0,2,4,6,8	1,3,5,7,9
	9	1	0,2,4,6,8,9	1,3,5,7,9,10
	10	1	0,2,4,6,8,10	1,3,5,7,9,11
	L^e	1	$0, 2, \dots, L$	$1, 3, \dots, L+1$
$\delta_c < \delta \leq 2\pi/L$	2	0	2	2
	3	0	3	3
	4	0	4	4
	5	0	5	5
	6	0	6	6
	7	0	7	7
	8	0	8	8
	9	0	9	9
	10	0	10	10
	L	0	L	L

^a n_o represents the number of pairs of DPs in MBZ with $k_x = 0$.
^b n_i represents the number of pairs of DPs in MBZ with $k_x = \pm\pi/3Lx$.

^c $n_t (= n_o + n_i)$ represents the total number of pairs of DPs in MBZ.

^d δ_c is a critical value where the number of DPs at the line $k_x = 0$ changes to zero. For $L_x = 2, 3, \dots, 10$, δ_c is approximately equal to $0.835\pi, 0.595\pi, 0.465\pi, 0.375\pi, 0.315\pi, 0.275\pi, 0.245\pi, 0.217\pi, 0.196\pi$, respectively.

^e $L \geq 2$. For L is an odd number, $n_i = 0, 2, 4, \dots, L-1, L$; for L is an even number, $n_i = 0, 2, 4, \dots, L$.

tion of the Fermi energy E_F . For $0 < \delta < \pi/2$ or $3\pi/2 < \delta < 2\pi$, the Hall conductivity can be expressed as $\sigma_{xy} = 4(N + 1/2)e^2/h$, which is the same as that of pristine graphene. This means that the Dirac-cone topology is preserved within this range without new induced DPs. For $\pi/2 < \delta < 2\pi/3$ or $4\pi/3 < \delta < 3\pi/2$, σ_{xy} has a $12e^2/h$ step across the zeroth LL and $4e^2/h$ or $8e^2/h$ step at the other LLs, implying the zeroth LL is 12-fold degenerate. Interestingly, for $2\pi/3 < \delta < 4\pi/3$, all LLs are 8-fold degenerate and the Hall conductivity can be expressed as $\sigma_{xy} = 8(N + 1/2)e^2/h$. This expression with quantized values of half-integer multiples of $8e^2/h$ is robust and is interpreted by the fact that the original pair of DPs has disappeared and the induced two pairs of DPs are located symmetrically in MBZ giving rise to exact 8-fold degeneracy of their corresponding LLs.

Thus far we have discussed two simplest SMFs where the magnetic flux alternates along the armchair chains or zigzag chains, respectively. Now we generalize our theory to the cases of SMF with long spatial period, shown in Fig. 1(c). Taking SMF-I for example, we make the magnetic flux alternate every L_x zigzag chains. Numerical analysis shows that, as δ increases from 0 to $2\pi/L_x$,³⁰ the number of pairs of original DPs n_o (at $k_x = 0$) de-

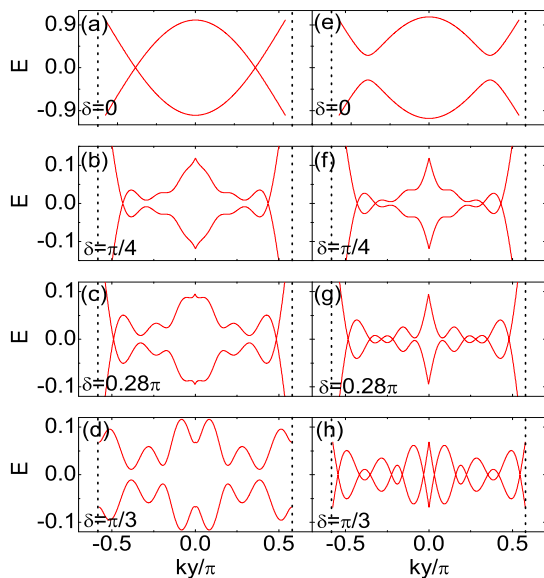


FIG. 6: (Color online) The case with $L_x = 6$. Electron energy near the DPs under a long-period SMF shown in Fig. 1 (c), as a function of k_y with (a)-(d) $k_x = 0$ and (e)-(f) $k_x = \pi/18$ for various values of staggered flux δ . The figures in (b),(f) and (c),(g) have been shifted to the left by 0.144π and 0.093π , respectively. The total number of pairs of DPs is 1,3,5,6, respectively for the four δ values.

creases from one to zero, while that of the induced DPs n_i (exactly located at the boundary of MBZ $k_x = \pm\pi/3L_x$) increases from zero to L_x gradually obeying a sequence of $0, 2, 4, \dots, L_x$. Accordingly, the total number of pairs of DPs is $n_t = 1, 3, 5, \dots, L_x + 1, L_x$. For the detail, see Table I. In Fig. 6, we take $L_x = 6$ for example. When $0 < \delta < 2\pi/L_x$, the number of pairs of the induced DPs shows a sequence of $n_i = 0, 2, 4, 6$ [Fig. 6(e)-(h)], while that of the original pair is always $n_o = 1$ or 0 [Fig. 6(a)-

(d)]. Once again, the DPs emerge and annihilate in pairs.

After application of such a long-period SMF, each pair of Dirac cones has generally different anisotropy, i.e., has different renormalization factor β in their corresponding LL spectrum, so all LLs except zeroth LL are still 4-fold degenerate. However, the zeroth LL is exact $4n_t$ -fold degenerate, leading to a step of size $4n_t e^2/h$ in σ_{xy} at the zeroth LL,³¹ as δ increasing from 0 to $2\pi/L_x$. Therefore, under a modulated orbital magnetic field, the property of neutral graphene is actually governed by the number of pairs of DPs. This is a significant signature and can be detected by Hall measurements. So long as L_x is no more than the magnetic length of the systems, the physics contained in them is similar. But for graphene system with the magnetic length much less than L_x , the DPs will become more and more dense and will finally be merged into the zeroth LL of graphene.²⁹ This deserve further study and will be discussed elsewhere.

In summary, we have investigated the electronic structure in neutral graphene under periodically modulated magnetic fields. It is found the modulated magnetic field can induce additional DPs in graphene and the evolution of these DPs can be manipulated by the magnitude and period of the field. These induced DPs add additional degeneracy to the LLs, especially a $4n_t$ -fold degeneracy at the zeroth LL, leading to an unusual integer QHE near neutral filling. These phenomena are expected to be observed by Hall measurements.

Acknowledgments

L. X. thanks Y. Zhou and Y. Zhao for useful discussion. This work was supported by NSFC Projects 10504009, 10874073 and 973 Projects 2006CB921802, 2006CB601002.

¹ F. D. M. Haldane, Phys. Rev. Lett. **61**, 2015 (1988).

² Y. Zheng and T. Ando, Phys. Rev. B **65**, 245420 (2002).

³ K. S. Novoselov, A. K. Geim, S. V. Morozov, D. Jiang, M. I. Katsnelson, I. V. Grigorieva, S. V. Dubonos, and A. A. Firsov, Nature (London) **438**, 197 (2005).

⁴ Y. Zhang, Y.-W. Tan, H. L. Stormer, and P. Kim, Nature (London) **438**, 201 (2005).

⁵ V. P. Gusynin, and S. G. Sharapov, Phys. Rev. Lett. **95**, 146801 (2005).

⁶ S. Y. Zhou, G.-H. Gweon, J. Graf, A. V. Fedorov, C. D. Spataru, R. D. Diehl, Y. Kopelevich, D.-H. Lee, S. G. Louie, and A. Lanzara, Nature Phys. **2**, 595 (2006)

⁷ D. N. Sheng, L. Sheng, and Z. Y. Weng, Phys. Rev. B **73**, 233406 (2006).

⁸ K. S. Novoselov, Z. Jiang, Y. Zhang, S. V. Morozov, H. L. Stormer, U. Zeilner, J. C. Maan, G. S. Boebinger, P. Kim, and A. K. Geim, Science **315**, 1379 (2007).

⁹ E. McCann, and V. I. Fal'ko, Phys. Rev. Lett. **96**, 086805 (2006).

¹⁰ K. S. Novoselov, E. McCann, S. V. Morozov, V. I. Fal'ko, M. I. Katsnelson, U. Zeilner, D. Jiang, F. Schedin, and A. K. Geim, Nature Phys. **2**, 177 (2006).

¹¹ J. Nilsson, A. H. Castro Neto, N. M. R. Peres, and F. Guinea, Phys. Rev. B **73**, 214418 (2006).

¹² C.-H. Park, L. Yang, Y.-W. Son, M. L. Cohen, and S. G. Louie, Nature Phys. **4**, 213 (2008); Phys. Rev. Lett. **101**, 126804 (2008).

¹³ M. Barbier, F. M. Peeters, P. Vasilopoulos, and J. M. Pereira, Jr., Phys. Rev. B **77**, 115446 (2008).

¹⁴ M. Ramezani Masir, P. Vasilopoulos, and F. M. Peeters, Phys. Rev. B **79**, 035409 (2009).

¹⁵ L. Dell'Anna, and A. De Martino, Phys. Rev. B **79**, 045420 (2009).

¹⁶ P. W. Sutter, J.-I. Flege, and E. A. Sutter, Nature Mater. **7**, 406 (2008).

¹⁷ A. L. Vázquez de Parga, F. Calleja, B. Borca, M. C. G. Passeggi, Jr., J. J. Hinarejos, F. Guinea, and R. Miranda, Phys. Rev. Lett. **100**, 056807 (2008).

- ¹⁸ D. Martoccia, P. R. Willmott, T. Brugger, M. Björck, S. Günther, C. M. Schlepütz, A. Cervellino, S. A. Pauli, B. D. Patterson, S. Marchini, J. Wintterlin, W. Moritz, and T. Greber, *Phys. Rev. Lett.* **101**, 126102 (2008).
- ¹⁹ I. Pletikosić, M. Kralj, P. Pervan, R. Brako, J. Coraux, A. T. N'Diaye, C. Busse, and T. Michely, *Phys. Rev. Lett.* **102**, 056808 (2009).
- ²⁰ J. C. Meyer, C. O. Girit, M. F. Crommie, and A. Zettl, *Appl. Phys. Lett.* **92**, 123110 (2008).
- ²¹ C.-H. Park, Y.-W. Son, L. Yang, M. L. Cohen, and S. G. Louie, *Phys. Rev. Lett.* **103**, 046808 (2009).
- ²² L. Brey and H. A. Fertig, *Phys. Rev. Lett.* **103**, 046809 (2009).
- ²³ G. Grynberg, B. Lounis, P. Verkerk, J.-Y. Courtois, and C. Salomon, *Phys. Rev. Lett.* **70**, 2249 (1993).
- ²⁴ C. Wu, D. Bergman, L. Balents, and S. Das Sarma, *Phys. Rev. Lett.* **99**, 070401 (2007).
- ²⁵ C. Wu, and S. Das Sarma, *Phys. Rev. B* **77**, 235107 (2008).
- ²⁶ M. Gibertini, A. Singha, V. Pellegrini, M. Polini, G. Vignale, A. Pinczuk, L. N. Pfeiffer, and K. W. West, *Phys. Rev. B* **79**, 241406 (2009).
- ²⁷ D. J. Thouless, M. Kohmoto, M. P. Nightingale, and M. den Nijs, *Phys. Rev. Lett.* **49**, 405 (1982).
- ²⁸ S. Banerjee, R. R. P. Singh, V. Pardo, and W. E. Pickett, *Phys. Rev. Lett.* **103**, 016402 (2009).
- ²⁹ L. Xu, J. An, and C.-D. Gong, arXiv:0912.2494
- ³⁰ Here we only consider the weak magnetic flux case $\delta < 2\pi/L_x$ for two reasons. One is the weak magnetic flux can be easily achieved in experiment; the other is that for strong magnetic flux, it is hard to find a good rule to describe the evolution of DPs.
- ³¹ The Hall plateaus are a little different from that discussed in Ref.21. In particular, when L_x is an even number, there is a $4L_x e^2/h$ Hall conductivity step.